

See discussions, stats, and author profiles for this publication at: <https://www.researchgate.net/publication/320821405>

# Structural characteristics of atmospheric temperature and humidity inside clouds of convective and stratiform precipitation in the rainy season over East Asia

Article in *Journal of Meteorological Research* · October 2017

DOI: 10.1007/s13351-017-7038-x

---

CITATIONS

4

2 authors:



Rui Wang  
Lanzhou University

8 PUBLICATIONS 23 CITATIONS

[SEE PROFILE](#)

---

READS

787



Yunfei Fu  
University of Science and Technology of China

179 PUBLICATIONS 2,394 CITATIONS

[SEE PROFILE](#)

Some of the authors of this publication are also working on these related projects:



Precipitation and Cloud Parameters in Summer Monsoon As Viewed by Satellite Instruments [View project](#)

## Structural Characteristics of Atmospheric Temperature and Humidity inside Clouds of Convective and Stratiform Precipitation in the Rainy Season over East Asia

Rui WANG<sup>1</sup> and Yunfei FU<sup>1,2,3\*</sup>

<sup>1</sup> School of Earth and Space Sciences, University of Science and Technology of China, Hefei 230026

<sup>2</sup> State Key Laboratory of Severe Weather, Chinese Academy of Meteorological Sciences, Beijing 100081

<sup>3</sup> Key Laboratory of Atmospheric Sciences and Satellite Remote Sensing of Anhui Province, Anhui Institute of Meteorological Sciences, Hefei 230031

(Received March 20, 2017; in final form June 15, 2017)

### ABSTRACT

In this study, a merged dataset constructed from Tropical Rainfall Measuring Mission precipitation radar rain products and Integrated Global Radiosonde Archive data is used to investigate the thermal structure characteristics of convective and stratiform precipitation in the rainy season (May–August) of 1998–2012 over East Asia. The results show that the storm tops for convective precipitation are higher than those for stratiform precipitation, because of the more unstable atmospheric movements for convective precipitation. Moreover, the storm tops are higher at 1200 UTC than those at 0000 UTC over land regions for both convective and stratiform precipitation, and vice versa for ocean regions. Additionally, temperature anomaly patterns inside convective and stratiform precipitating clouds show a negative anomaly of about 0–2 K, which results in cooling effects in the lower troposphere. This cooling is more obvious at 1200 UTC for stratiform precipitation. The positive anomaly that appears in the middle troposphere is more than 2 K, with the strongest warming at 300 hPa. Relative humidity anomaly patterns show a positive anomaly in the middle troposphere (700–500 hPa) prior to the two types of precipitation, and the increase in moisture is evident for stratiform precipitation.

**Key words:** vertical structure of precipitation, atmospheric stability, temperature anomaly, relative humidity anomaly

**Citation:** Wang, R., and Y. F. Fu, 2017: Structural characteristics of atmospheric temperature and humidity inside clouds of convective and stratiform precipitation in the rainy season over East Asia. *J. Meteor. Res.*, **31**(5), 1–16, doi: 10.1007/s13351-017-7038-x.

### 1. Introduction

Traditionally, rain gauge observations or ground-based weather radar detections are used to obtain rain rates or three-dimensional (3D) rain echoes of precipitating clouds. Meanwhile, advanced satellite-borne precipitation radar, such as the earlier Tropical Rainfall Measuring Mission (TRMM) precipitation radar (PR) and the more recent Global Precipitation Measurement Dual-frequency Precipitation Radar (DPR), can homogeneously measure precipitating clouds on a larger scale, providing the rain rate and 3D precipitation structures of precipitating clouds associated with their spatiotemporal distribution for different precipitation types, such as convective and stratiform precipitation (Liu and Fu, 2001;

Fu and Liu, 2003; Fu et al., 2013). The vertical structure of precipitation obtained from PR or DPR is very useful in retrieving the latent heat released through cloud precipitation processes (Li et al., 2013). Currently, satellite-derived observational products are used into many studies (e.g., Zhou and Wang, 2006; Houze et al., 2007; Li et al., 2012; Qin and Fu, 2016).

On the other hand, the vertical atmospheric temperature and humidity measured by the Integrated Global Radiosonde Archive (IGRA) offer substantially higher vertical resolution than reanalysis, as well as much longer records than GPS radio occultation, and has thus supplied an essential dataset in analyzing and understanding the vertical structures of temperature and humidity at the global scale (Durre et al., 2006). For example, Alexeev et

Supported by the National Natural Science Foundation of China (91337213, 41230419, and 41505033) and China Meteorological Administration Special Public Welfare Research Fund (GYHY201406001 and GYHY201306077).

\*Corresponding author: fyf@ustc.edu.cn.

©The Chinese Meteorological Society and Springer-Verlag Berlin Heidelberg 2017

al. (2012) evaluated the Arctic temperature trend around 1990 using IGRA. They found that the temperature changed from negative to positive in the lower stratosphere (200–70 hPa). Based on IGRA, Feng et al. (2012) analyzed the global trend in the thickness of the tropopause layer during 1965–2004. The results revealed that the tropopause layer thickened during this period, with a positive trend of  $0.16 \pm 0.12 \text{ km (10 yr)}^{-1}$ .

Combining radiosonde sounding and TRMM products, Folkins et al. (2008) found that deep convection cooled the atmosphere in the lower troposphere of equatorial regions over a horizontal distance of about 1000 km. Using TRMM 3B42 products and IGRA, Mitovski and Flokins (2014) indicated that regional similarities and differences in the interaction between high rainfall events and the background atmosphere from 1998 to 2010. Xian and Fu (2015) revealed that the frequency of tropopause-penetrating convection decreased exponentially with height in the tropics, based on TRMM PR data together with Constellation Observing System for Meteorology, Ionosphere, and Climate data.

Nevertheless, knowledge about the vertical structure of atmospheric temperature and humidity inside precipitating clouds, such as convective and stratiform precipitation, remains insufficient. This is the motivation behind the present study, in which we focus on the characteristics of atmospheric temperature and humidity inside precipitating clouds over the East Asian summer monsoon (EASM) region, where the characteristics of precipitation are strongly affected by the local topography. According to previous studies (Zhou et al., 2008; Bao et al., 2011; Zhu et al., 2011; Xu, 2013), four regions are selected: the Sichuan basin (SCB;  $28.0^{\circ}\text{--}32.0^{\circ}\text{N}$ ,  $102.0^{\circ}\text{--}110.0^{\circ}\text{E}$ ), Southeast China (SEC;  $23.0^{\circ}\text{--}26.0^{\circ}\text{N}$ ,  $112.5^{\circ}\text{--}118.5^{\circ}\text{E}$ ), middle-eastern China (MEC;  $28.0^{\circ}\text{--}32.0^{\circ}\text{N}$ ,  $112.5^{\circ}\text{--}123.0^{\circ}\text{E}$ ) and the Northwest Pacific (NWP;  $25.0^{\circ}\text{--}29.0^{\circ}\text{N}$ ,  $127.5^{\circ}\text{--}142.5^{\circ}\text{E}$ ), as shown in Fig. 1.

Following this introduction, the data and methodology are described in Section 2. The water vapor transport, vertical structure of convective and stratiform precipitation, atmospheric stability, temperature, and relative humidity anomaly patterns inside convective and stratiform precipitating clouds are explored in Section 3. Meanwhile, the interactions between precipitation and these atmospheric parameters are also discussed in this section. Section 4 summarizes and draws conclusions from the study.

## 2. Data and methodology

The TRMM PR 2A25 version 7 products issued by the

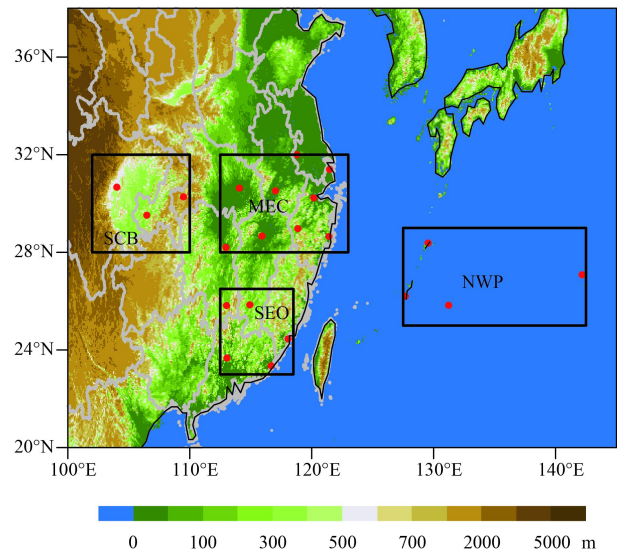


**Fig. 1.** Topography of the East Asian summer monsoon region (shaded) and the IGRA stations (red solid circles) in four regions of East Asia (SCB, Sichuan basin; SEC, Southeast China; MEC, middle-eastern China; NWP, Northwest Pacific).

Goddard Space Flight Center (GSFC) are used to investigate the vertical structure of convective and stratiform precipitation over the EASM region from 1998 to 2012. These products provide precipitation information, including location, scanning time, precipitation type and 3D radar reflectivity from the surface to 20 km, with a horizontal resolution of 4.3 km and a vertical resolution of 0.25 km (Kummerow et al., 1998). Owing to the orbit boost of TRMM after August 2001, the detection threshold of PR is 17 dBZ in radar reflectivity and 0.4 mm h<sup>-1</sup> in rain rate (Schumacher and Houze, 2003). Consequently, in this study, only PR 2A25 pixels with radar reflectivity larger than 17 dBZ and a rain rate greater than 0.4 mm h<sup>-1</sup> at near-surface layer are included.

To obtain the structures of atmospheric stability associated with temperature and humidity for convective and stratiform precipitation, the IGRA data archived at the National Climatic Data Center (NCDC) are used. These data provide the pressure, temperature, dew-point temperature, geopotential height, and other meteorological parameters at standard levels. The data are subjected to rigorous quality control and are measured twice daily (0000 and 1200 UTC) (Durre et al., 2006). Considering the period of overlap between TRMM PR and IGRA, IGRA data from 1998 to 2012 are selected. Moreover, missing data at each individual IGRA station should be less than 20% (Guo and Ding, 2009).

To analyze the water vapor transport in the rainy season from 1998 to 2012, reanalysis data obtained from NCEP at 0000 and 1200 UTC are selected, including ho-

horizontal wind and specific humidity with a horizontal resolution of  $2.5^\circ$  at 850 hPa.

To investigate the atmospheric structures of temperature and humidity for convective and stratiform precipitation, we merge the PR 2A25 products with the IGRA dataset from 1998 to 2012. The location and sounding time of IGRA observations are fixed, whereas the geographical location and scanning time of rain pixels measured by PR vary with TRMM PR orbit positions. Therefore, it is necessary to match both datasets in time and space. As suggested by Xia and Fu (2016), it is practicable to match the PR 2A25 and IGRA data at each IGRA station within its  $0.25^\circ$  grid before and after two hours of IGRA observations. Ultimately, a new dataset with quasi spatiotemporal synchronization is established for our study. Note that the atmospheric profiles from IGRA represent the mean state of the atmosphere for temperature and dew-point temperature during the period of observation, rather than the instantaneous state; whereas, the precipitation profiles from TRMM PR represent the instantaneous state of precipitation structure.

In this paper, convective (stratiform) precipitation is defined where convective (stratiform) pixels comprise more than 30% (70%) of the total pixels in each PR sample. Table 1 shows samples of IGRA classified as un-

der convective or stratiform precipitation and the associated precipitating pixels detected by PR. The samples are statistically sufficient in each selected region. Clearly, the numbers of samples for stratiform precipitation at 0000 and 1200 UTC are more than those for convective precipitation, which is consistent with previous studies (Fu et al., 2007, 2008).

### 3. Results

#### 3.1 Water vapor transport in the rainy season over the EASM region

It is well-known that the variation in precipitation is influenced by general circulation over the EASM region (Ding et al., 2008). Therefore, before studying the structure of precipitation, we examine the water vapor transport at 850 hPa in the rainy season. As shown in Fig. 2, water vapor comes from different directions and has different influences in the four regions. SCB is dominated by southeasterly water vapor transport. Meanwhile, there are two different branches of water vapor transport in SEC and MEC, one is southerly from the East China Sea, and the other is northerly from the area of Bohai or Huanghai. Water vapor from the western Pacific converges over the NWP. These results are consistent with previous

**Table 1.** IGRA and TRMM PR 2A25 samples for convective and stratiform precipitation in the rainy season during 1998–2012 in four regions of East Asia

	0000 UTC				1200 UTC			
	Convective		Stratiform		Convective		Stratiform	
IGRA	PR 2A25	IGRA	PR 2A25	IGRA	PR 2A25	IGRA	PR 2A25	
SCB	67	981	161	3827	108	852	135	2246
SEC	162	1856	190	3912	176	2694	250	5826
MEC	266	3555	510	12820	302	3351	510	10866
NWP	165	1395	173	4048	140	912	168	3865

Note: SCB, Sichuan basin; SEC, Southeast China; MEC, middle-eastern China; NWP, Northwest Pacific

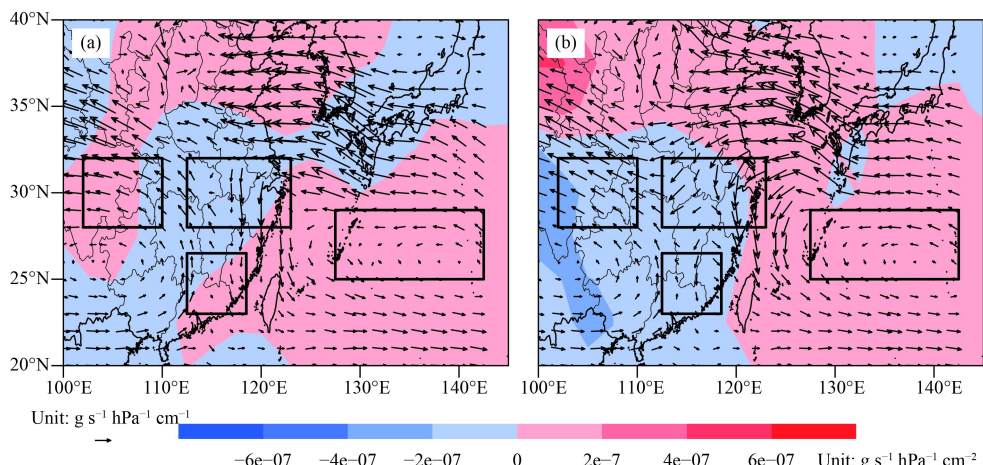


**Fig. 2.** Mean 850-hPa moisture flux field ( $\text{g s}^{-1} \text{hPa}^{-1} \text{cm}^{-1}$ ) superimposed on the moisture flux divergence field ( $\text{g s}^{-1} \text{hPa}^{-1} \text{cm}^{-2}$ ) at (a) 0000 UTC and (b) 1200 UTC over the EASM region during 1998–2012.

studies (Fu et al., 2005; Zhou and Yu, 2005). Water vapor transport drives warm and moist air from the ocean to the land regions (SCB, SEC, and MEC) in the lower troposphere, which provides sufficient moisture for precipitation over the EASM region. In addition, the moisture flux divergence field at 850 hPa over the EASM region is shown by the shading in Fig. 2. A negative (positive) moisture flux divergence indicates water vapor convergence (divergence) (Juneng and Tangang, 2005), and water vapor convergence is conducive to the formation of precipitation (Liu et al., 2005). Significant water vapor convergence exists in SCB, SEC, and MEC at 1200 UTC, whereas water vapor divergence exists in NWP. Moreover, the convergence intensity of the water vapor at 1200 UTC is stronger than that at 0000 UTC in SCB and SEC, which could enhance the formation of precipitation in these two regions at 1200 UTC.

### 3.2 Precipitation cases

To preliminarily check the results of the merged dataset and demonstrate the thermal structure and the vertical structure of precipitation inside precipitating clouds in SCB, SEC, MEC, and NWP, eight typical precipitation cases that occurred around IGRA stations located in the four regions are chosen from the merged data. Some basic information regarding these precipitation cases is listed in Table 2.

The contoured frequency by altitude diagrams (CFADs) of TRMM PR reflectivity reflect the characteristics of the radar reflectivity frequency and storm top (Yuter and Houze, 1995; Lang et al., 2003). CFADs for the four precipitation cases are presented in Fig. 3. The vertical structures of convective precipitation at Enshi, Ganzhou, Wuhan, and Naha stations are shown in Figs. 3a–d, respectively. The PR reflectivity is larger than 50 dBZ within 2–5 km. Moreover, the vertical development of precipitation is deep at these four stations, and the storm tops are higher than 10 km. In contrast, the CFADs show vertical structures of stratiform precipitation at Chongqing, Xiamen, Changsha, and Chichi Jima stations, in Figs. 3e–h. The PR reflectivity is less than 45

dBZ, and the storm tops are lower than 10 km. The vertical development of precipitation is shallow.

To explore the vertical structure of temperature and moisture inside convective and stratiform precipitating clouds, skew-T-logp diagrams are shown in Fig. 4. Clearly, the dew-point temperature profiles of the precipitation cases are close to the temperature profiles in the lower troposphere, which suggests that the atmosphere is close to saturation. However, the dew-point temperature profiles drift left during ascent, especially in the upper troposphere (Figs. 4a–h). This suggests that the depression of the dew-point is small in the lower troposphere and large in the upper troposphere. In other words, the atmosphere is moister in the lower troposphere during the precipitation process.

### 3.3 Statistical analysis

#### 3.3.1 Vertical structure of convective and stratiform precipitation

The characteristics of the vertical structure of precipitation and thermal structure inside precipitating clouds in the four regions in the rainy season from 1998 to 2012 are presented through statistical analysis in this section. Like Fig. 3, Figs. 5 and 6 show twice-daily (0000 and 1200 UTC) CFADs for convective and stratiform precipitation in the four regions. According to Fig. 5, the storm top is higher than 10 km in the four regions, both at 0000 and 1200 UTC. The storm tops even exceed 15 km in SCB and MEC at 1200 UTC. Notably, the storm tops in the land areas (SCB, SEC, and MEC) are higher than those in the ocean area (NWP). Additionally, a large frequency of PR reflectivity, 20%–40%, gradually shifts to the right side of the CFADs from the storm top to 4 km. That is, radar reflectivity observed by PR becomes larger, because rain particles grow larger during descent (Houze, 1997; Fu et al., 2008). Compared with convective precipitation, stratiform precipitation develops more shallowly (Fig. 6). The radar storm tops are similar in the four regions. Moreover, from the height of the storm top to 10 km, the radar reflectivity of stratiform precipitation is mainly 20 dBZ. From 10 km down to 5 or 6 km, the

**Table 2.** Details of the precipitation cases chosen to assess the merged dataset

Region	Type	Station	IGRA (UTC)	PR (UTC)
SCB	Convective	Enshi (57447) (30.27°N, 109.48°E)	2011.07.21 23:00	2011.07.21 21:00
SCB	Stratiform	Chongqing (57516) (29.52°N, 106.48°E)	2008.06.14 23:00	2008.06.15 00:00
SEC	Convective	Ganzhou (57993) (25.85°N, 114.93°E)	2001.08.29 11:00	2001.08.29 09:00
SEC	Stratiform	Xiamen (59134) (24.45°N, 118.07°E)	2006.05.15 23:00	2006.05.16 01:00
MEC	Convective	Wuhan (57494) (30.63°N, 114.07°E)	2001.06.17 23:00	2001.06.17 22:00
MEC	Stratiform	Changsha (57679) (28.2°N, 112.97°E)	2006.07.26 11:00	2006.07.26 13:00
NWP	Convective	Naha (47936) (26.2°N, 127.68°E)	2006.08.06 00:00	2006.08.06 01:00
NWP	Stratiform	Chichi Jima (47971) (27.08°N, 142.18°E)	2007.05.21 00:00	2007.05.20 22:00

Note: SCB, Sichuan basin; SEC, Southeast China; MEC, middle-eastern China; NWP, Northwest Pacific.

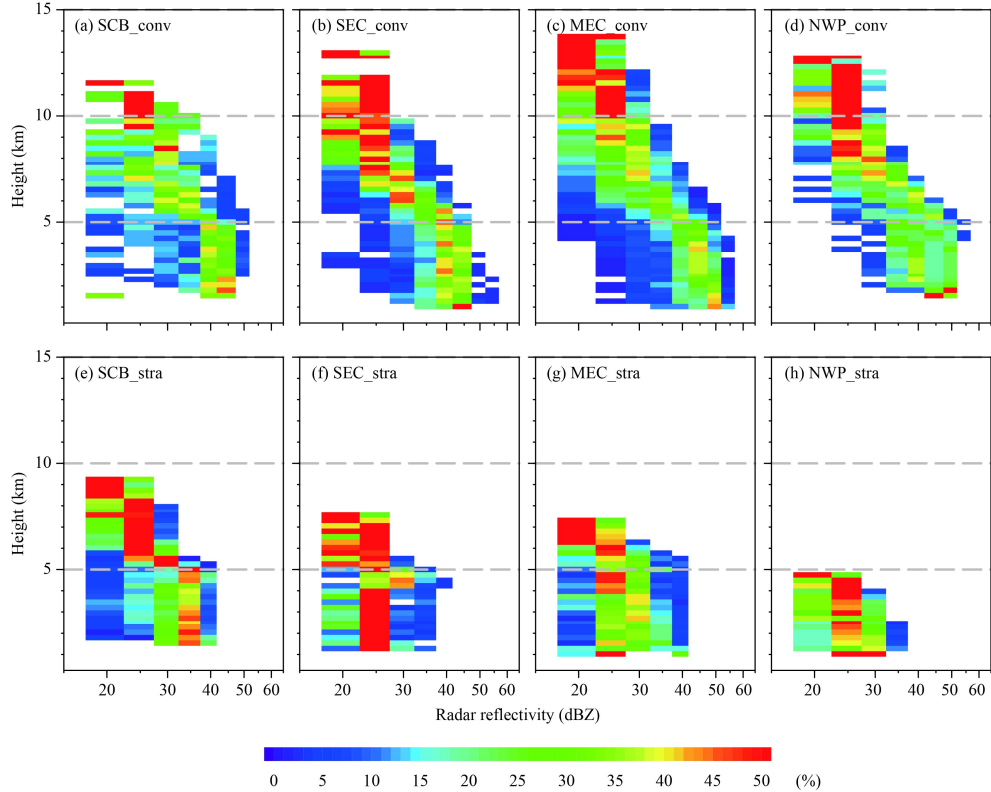


**Fig. 3.** Contoured frequency by altitude diagrams of TRMM PR reflectivity of precipitation cases in four regions: (a) Enshi, (b) Ganzhou, (c) Wuhan, (d) Naha, (e) Chongqing, (f) Xiamen, (g) Changsha, and (h) Chichi Jima.

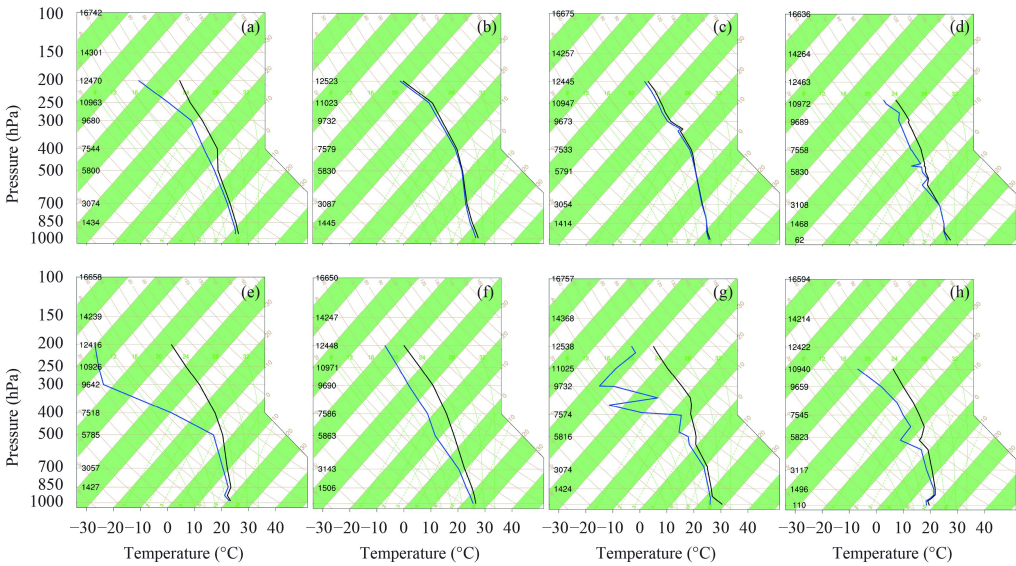


**Fig. 4.** Skew-T-logp diagrams of precipitation cases: (a) Enshi; (b) Ganzhou; (c) Wuhan; (d) Naha; (e) Chongqing; (f) Xiamen; (g) Changsha; (h) Chichi Jima. Black solid lines show the temperature profiles and blue solid lines show the dew-point temperature profiles.

radar reflectivity mainly ranges from 20–40 dBZ, increasing with descent. Below 5 km, the distribution of the CFAD changes little with height. In conclusion, the maximum value of radar reflectivity occurs near 5 or 6 km. Therefore, the characteristics of the 0°C melting

level (5–6 km) are evident. Furthermore, the storm tops are higher at 1200 UTC than at 0000 UTC (Figs. 5 and 6) over the land regions (SCB, SEC, and MEC), for both types of precipitation, because peak rainfall of convective and stratiform precipitation occurs usually in the af-

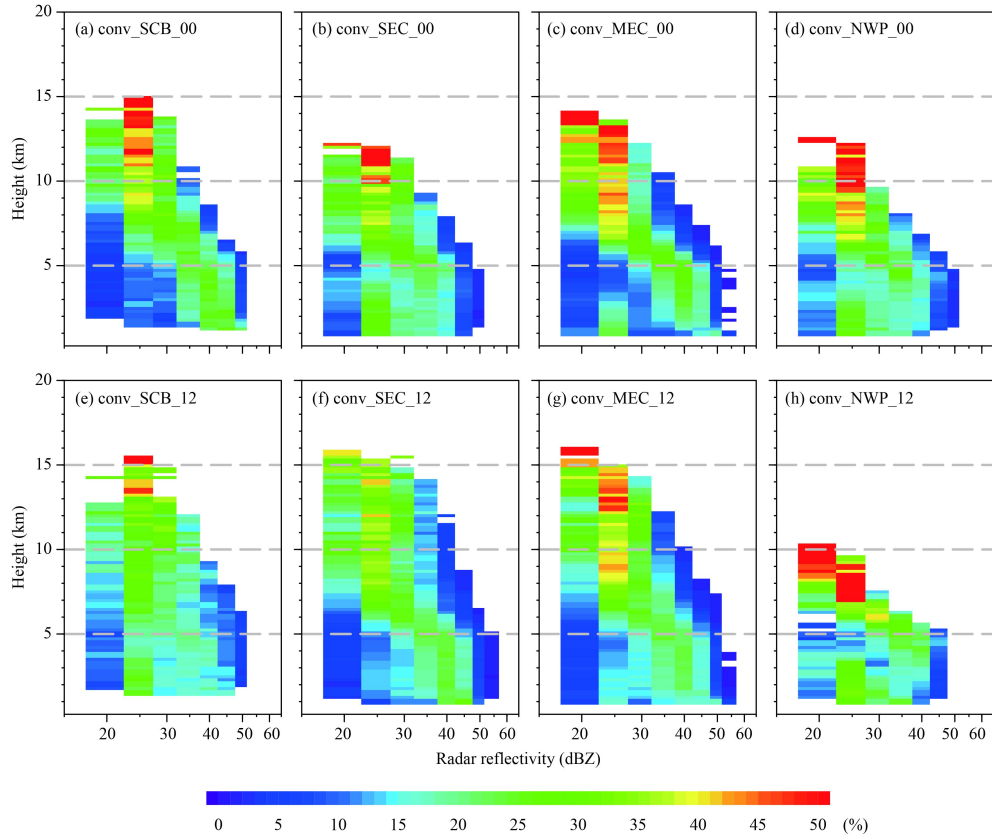


**Fig. 5.** CFADs of TRMM PR reflectivity of convective precipitation in four regions of East Asia (SCB, Sichuan basin; SEC, Southeast China; MEC, middle-eastern China; NWP, Northwest Pacific).

ternoon over land (Nesbitt and Zipser, 2003; Yu et al., 2007; Fu et al., 2017). Peak rainfall for convective precipitation occurs in the afternoon or evening (1200 UTC) over SEC and MEC, but over SCB nighttime rain occurs frequently (Yu et al., 2007; Liu and Fu, 2010). Meanwhile, peak rainfall occurs in the morning over the ocean area (NWP) (Fu et al., 2012). Therefore, the storm tops are higher at 1200 UTC in SEC and MEC, and higher at 0000 UTC in NWP.

To analyze the magnitude of the near-surface rain rate, the corresponding probability density functions (PDFs) of the near-surface rain rate for convective and stratiform precipitation in the four regions are shown in Fig. 7. The results show that the distributions of the PDFs for convective precipitation are “wide”, and the maximum rain rate can reach  $20 \text{ mm h}^{-1}$  (Figs. 7a, c). In addition, the total area fractions of PDFs with a rain rate less than  $5 \text{ mm h}^{-1}$  for convective precipitation over the ocean region (NWP) are larger than those over the land regions (SCB, SEC, and MEC), whereas the total area fractions with rain rates larger than  $5 \text{ mm h}^{-1}$  over the land regions exceed those over the ocean region. The distributions of PDFs for stratiform precipitation are similar in

the four regions, and the near-surface rain rates are less than  $10 \text{ mm h}^{-1}$  (Figs. 7b, d). As shown in Table 3, the mean near-surface rain rate at 0000 UTC in SCB, SEC, MEC, and NWP is  $9.0, 6.3, 9.4$ , and  $6.0 \text{ mm h}^{-1}$ , respectively, for convective precipitation; and  $1.8, 2.3, 1.9$ , and  $3.1 \text{ mm h}^{-1}$  for stratiform precipitation. Additionally, the mean near-surface rain rate at 1200 UTC is  $7.5, 8.0, 9.6$ , and  $4.9 \text{ mm h}^{-1}$  for convective precipitation; and  $1.5, 1.9, 1.8$ , and  $1.9 \text{ mm h}^{-1}$  for stratiform precipitation. The maximum near-surface rain rate for convective precipitation occurs early in the morning in SCB (Yu et al., 2007; Liu and Fu, 2010). Thus, the mean surface rain rate at 0000 UTC is larger than that at 1200 UTC in this region. As a result, a higher storm top does not correspond to a larger near-surface rain rate in SCB. However, the storm tops for convective precipitation are higher at 1200 UTC than at 0000 UTC in SEC and MEC, which corresponds to larger near-surface rain rates at 1200 UTC. Similarly, a higher storm top corresponds to a larger near-surface rain rate at 0000 UTC in NWP. Therefore, the storm tops for convective precipitation increase with an increment in the near-surface rain rate in SEC, MEC, and NWP (Fu et al., 2005, 2012; Chen et al., 2016). As for stratiform pre-

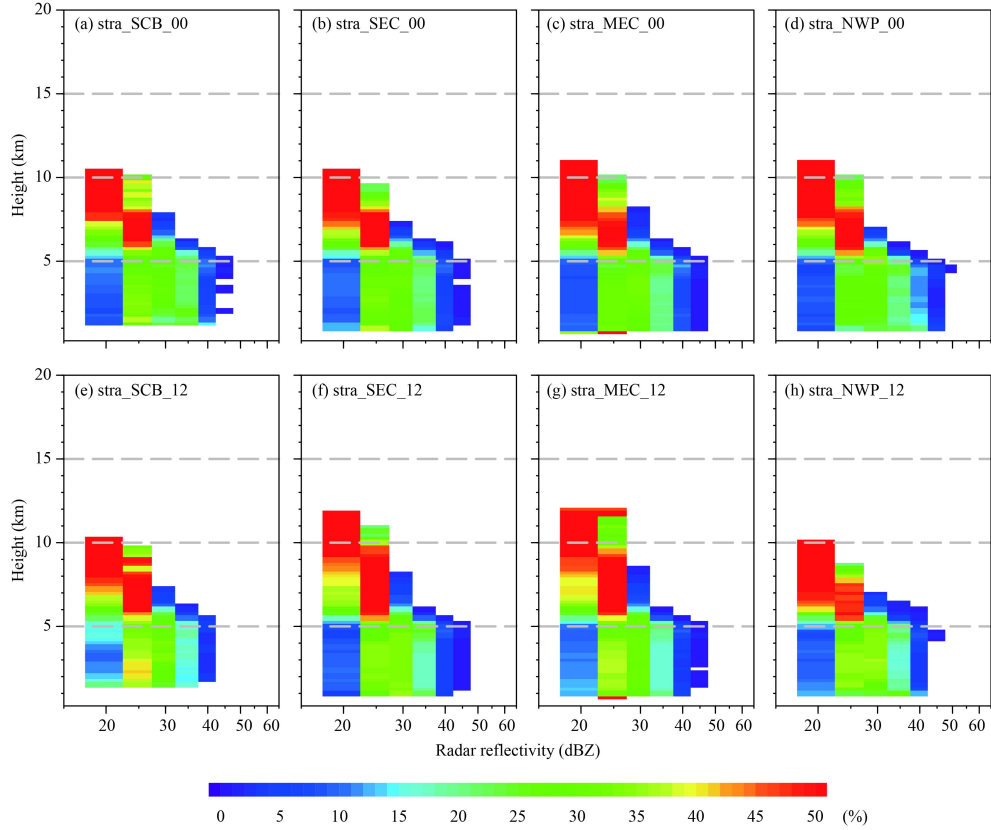


**Fig. 6.** As in Fig. 5, but for stratiform precipitation.

cipitation, the near-surface rain rates at 0000 UTC are larger than the values at 1200 UTC in SCB, SEC, and MEC, which is a different result to that of convective precipitation. Consequently, the storm tops for stratiform precipitation do not increase with the near-surface rain rate over the land regions (SCB, SEC, and MEC).

A rain rate profile exhibits the strength of the vertical movement as well as the microphysical processes of precipitation, and the slope of the rain rate profile reveals the latent heat release (Fu et al., 2005; Liu et al., 2013). Figure 8 shows the rain rate profiles of convective and stratiform precipitation at 0000 and 1200 UTC. The mean storm tops for convective and stratiform precipitation in the four regions are coincident with the results in Figs. 5, 6. For convective precipitation (Figs. 8a, c), the rain rate increases towards the surface, which results from the increasing sizes of raindrops during descent (Liu and Fu, 2001; Fu et al., 2017). For stratiform precipitation (Figs. 8b, 8d), the rain intensity reaches its maximum value rapidly below the 0°C melting level (5–6 km), and a larger value occurs in NWP. The shapes of the rain rate profiles for convective and stratiform precipitation in Figs. 8c and 8d are similar to those in Figs. 8a and 8b, respectively. However, the rain intensity of convective precipitation at 1200 UTC is larger than that at

0000 UTC in SEC and MEC. The rain intensity of stratiform precipitation at 0000 UTC is larger in the four regions, which shows consistency with the results in Table 3.

### 3.3.2 Atmospheric stability distribution for convective and stratiform precipitation

Unstable stratification of the atmosphere is necessary for precipitation (Adams and Souza, 2009; Lu et al., 2016), and the atmospheric Emagram is commonly used to analyze the atmospheric stability based on sounding observations (Sheng et al., 2003). In an Emagram, the two points where the stratification curve and state curve cross denote the level of free convection (LFC) and the level of neutral buoyancy (LNB), respectively. Generally, air parcels are influenced by the external environment and lifted adiabatically from the LFC to the LNB. The positive area integrated from the stratification curve to the state curve from the LFC to the LNB denotes the magnitude of unstable atmospheric energy. Moreover, the depth from the LFC to the LNB not only denotes the intensity of convective activity, but also the average magnitude of upward air buoyancy, which affects the formation and development of precipitation (Iturrioz et al., 2007; Zheng et al., 2008; Masunaga, 2012; Ratnam et al., 2013).

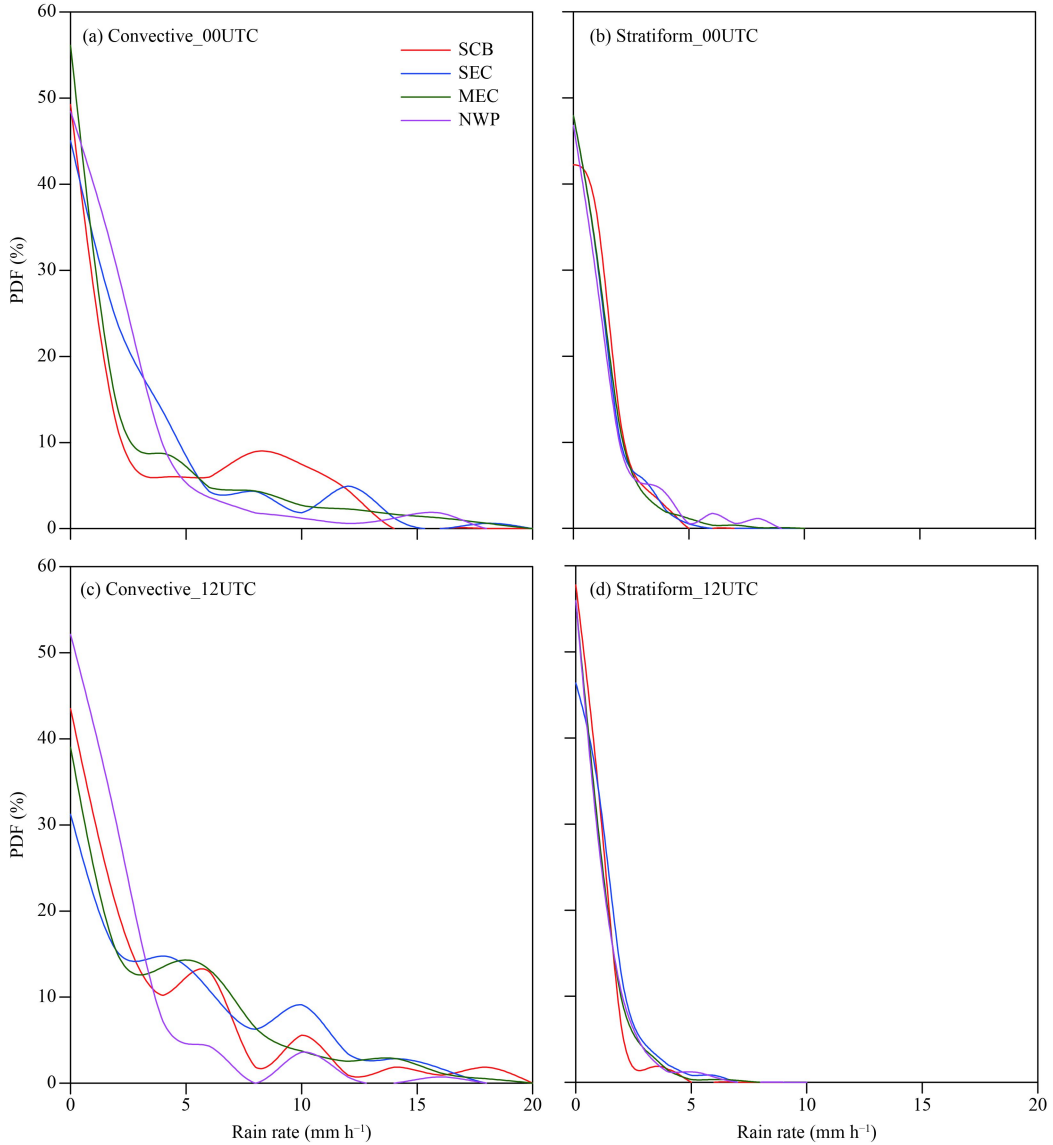


**Fig. 7.** PDFs of near-surface rain rate for convective and stratiform precipitation in four regions of East Asia (SCB, Sichuan basin; SEC, Southeast China; MEC, middle-eastern China; NWP, Northwest Pacific).

**Table 3.** Mean near-surface rain rate ( $\text{mm h}^{-1}$ ) for convective and stratiform precipitation at 0000 UTC and 1200 UTC in four regions

	0000 UTC		1200 UTC	
	Convective	Stratiform	Convective	Stratiform
SCB	9.0	1.8	7.5	1.5
SEC	6.3	2.3	8.0	1.9
MEC	9.4	1.9	9.6	1.8
NWP	6.0	3.1	4.9	1.9

Note: SCB, Sichuan basin; SEC, Southeast China; MEC, middle-eastern China; NWP, Northwest Pacific.

Based on the principle of the Emagram, the positive area frequency is the two-dimensional PDF calculated between the stratification curve and state curve from the LFC to the LNB. Figure 9 shows the distribution of positive area frequency for convective precipitation, in which the tops of the positive area at 1200 UTC reach

150 hPa — higher than those at 0000 UTC (200 hPa) over the land regions (SCB, SEC and MEC). This result implies that vertical movements develop higher at 1200 UTC. Comparing Fig. 5 with Fig. 9, the relationship between the vertical development of convective precipitation and vertical atmospheric movements can be analyzed. The results show that higher storm tops correspond to stronger upward movements over the land regions, which suggests that the vertical development of precipitation depends on strong upward movement due to unstable energy. Furthermore, the distribution of positive area frequency for stratiform precipitation (Fig. 10) is similar to that for convective precipitation (Fig. 9). However, the tops of the positive area for convective precipitation are relatively higher than those for stratiform

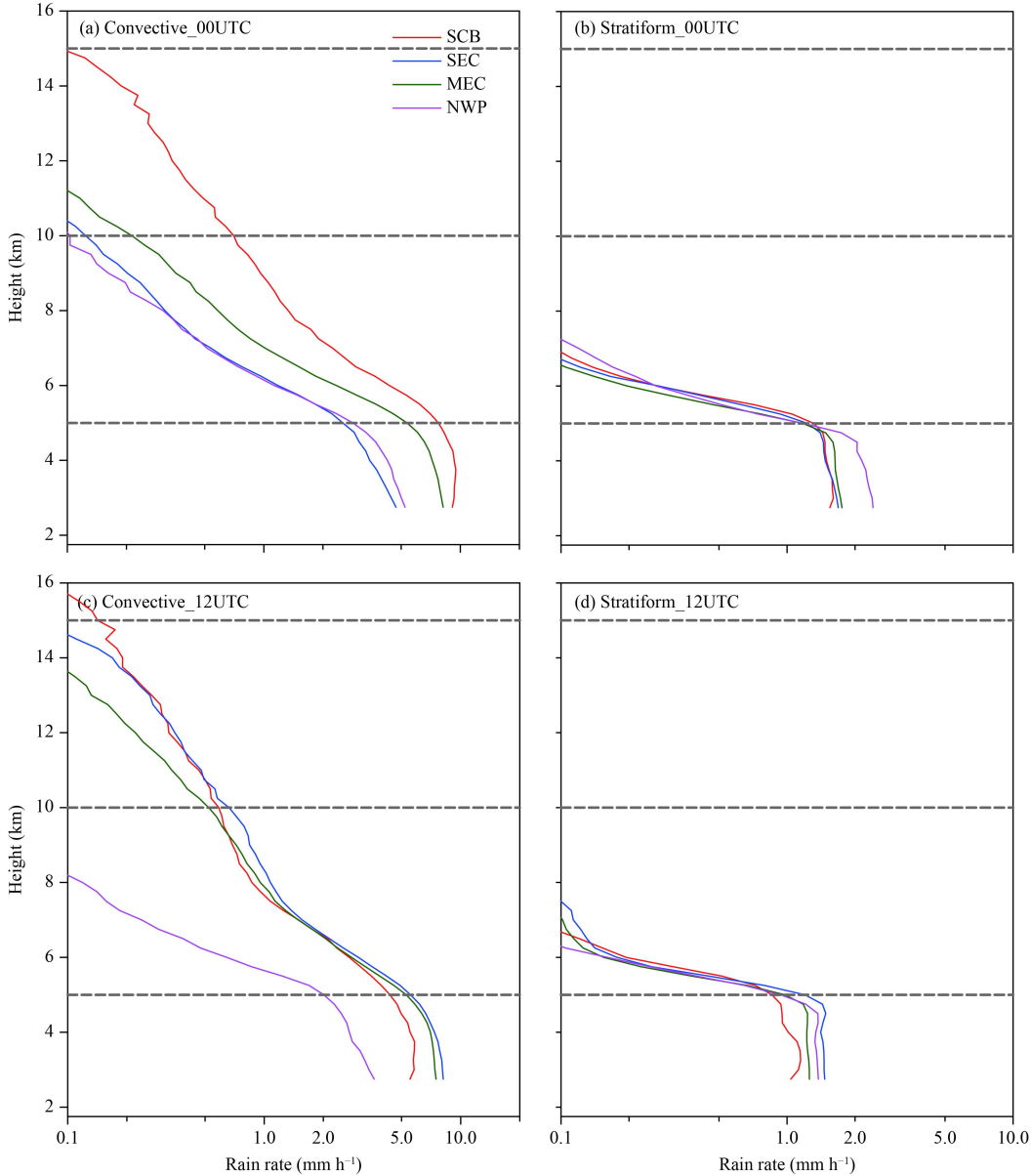


**Fig. 8.** Mean profiles of rain rate for convective and stratiform precipitation in four regions of East Asia (SCB, Sichuan basin; SEC, Southeast China; MEC, middle-eastern China; NWP, Northwest Pacific).

precipitation, which corresponds to higher storm tops for convective precipitation in the four regions.

Additionally, the temperature profiles are close to the dew-point profiles in the lower troposphere (Figs. 9, 10). Specifically, the depression of the dew point is small, which indicates the lower troposphere is moist in the four regions during the precipitation process. To reveal the difference in temperature and dew point in detail, Table 4 shows the mean depression of the dew point (DDP) near the surface in the four regions. The DDP is smaller at 0000 UTC than at 1200 UTC near the surface over the land regions (SCB, SEC, and MEC), for both convective and stratiform precipitation. That is, the atmosphere is

moister at 0000 UTC over the land regions near the surface. The opposite result is found over the ocean region (NWP). Moreover, the DDP for stratiform precipitation is smaller than that for convective precipitation at the same time point. This suggests that the atmosphere is moister during stratiform precipitation. Table 5 shows the DDP results for the middle troposphere (500 hPa), revealing that the DDP at this level is significantly larger than the DDP near the surface at the same time point and for the same precipitation type (except stratiform precipitation at 1200 UTC in SCB). Therefore, it can be concluded that the atmosphere is moister in the lower troposphere and drier in the upper troposphere during the pre-

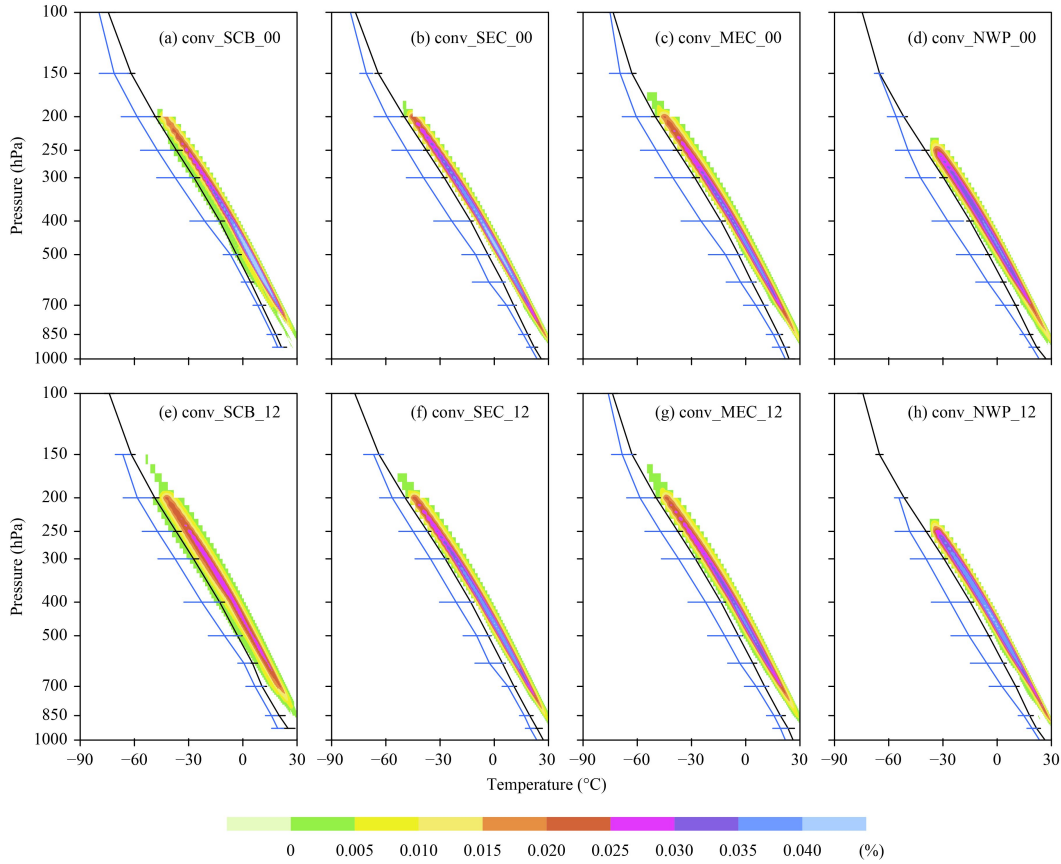


**Fig. 9.** Positive Area frequency (color shading) corresponding to the mean temperature profile (black solid line) and dew-point temperature profile (blue solid line) for convective precipitation in the rainy season during 1998–2012 in four regions of East Asia (SCB, Sichuan basin; SEC, Southeast China; MEC, middle-eastern China; NWP, Northwest Pacific).

cipitation process.

Table 6 shows the average convective available potential energy (CAPE) for convective and stratiform precipitation at 0000 and 1200 UTC in the four regions. Generally, CAPE values for convective precipitation are larger than those for stratiform precipitation in the four regions. This result suggests that the atmospheric stability is more unstable when convective precipitation occurs. Therefore, the storm tops for convective precipitation are higher than those for stratiform precipitation, due to more unstable atmospheric movements. Moreover, CAPE values are larger at 1200 UTC than at 0000 UTC, for both types of precipitation, in SCB, SEC, and MEC; whereas, CAPE is larger at 0000 UTC than at 1200 UTC in NWP. This indicates that the atmosphere is more unstable in the evening (1200 UTC) over land regions, while the atmosphere is more unstable in the morning over the ocean region. Of note is that CAPE values over the ocean region (NWP) are larger than those over the land regions (SCB, SEC, and MEC). However, evaporative cooling occurs over the ocean and restrains the development of updrafts (Wu et al., 2013). Moreover, the higher surface elevation

over land regions may give rise to dynamic forcing (Yu et al., 2014; Fu et al., 2017). Consequently, storm tops over land regions develop higher than those over the ocean.

### 3.3.3 Temperature and relative humidity anomaly structure inside convective and stratiform precipitating clouds

The process of the precipitation is associated with the atmospheric temperature and relative humidity (Rosenfeld and Lensky, 1998). To examine the structure of temperature and relative humidity inside convective and stratiform precipitating clouds, the merged TRMM PR 2A25 and IGRA data are used to calculate the temperature and relative humidity anomaly from 12 h prior to the precipitation process to 12 h after.

The temperature anomaly relates to the vertical atmospheric movement during the period of precipitation (Sheng et al., 2003). That is, a positive anomaly suggests upward movement, whereas a negative anomaly suggests downdraft. As illustrated in Fig. 11 for convective precipitation, the temperature anomaly is negative in the lower troposphere, which corresponds to downdrafts, and

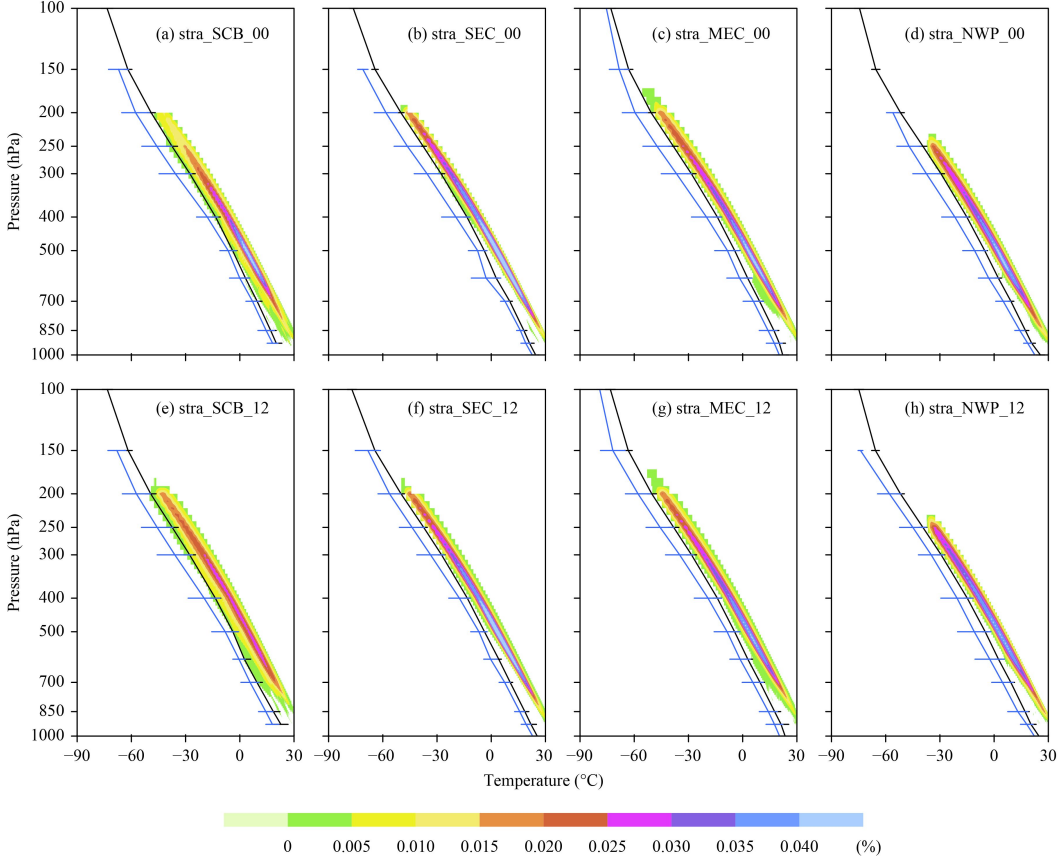


**Fig. 10.** As in Fig. 9, but for stratiform precipitation.

**Table 4.** Mean depression of the dew point ( $^{\circ}$ C) for convective and stratiform precipitation near the surface in the rainy season during 1998–2012 in four regions of East Asia

		SCB	SEC	MEC	NWP
Convective	Near surface (0000 UTC)	2.1	2.3	2.1	3.9
	Near surface (1200 UTC)	5.7	3.6	4.3	3.0
Stratiform	Near surface (0000 UTC)	2.0	1.9	1.9	3.1
	Near surface (1200 UTC)	4.7	2.6	3.1	2.5

Note: SCB, Sichuan basin; SEC, Southeast China; MEC, middle-eastern China; NWP, Northwest Pacific.

**Table 5.** Mean depression of the dew point ( $^{\circ}$ C) for convective and stratiform precipitation at 500 hPa in the rainy season during 1998–2012 in four regions of East Asia

		SCB	SEC	MEC	NWP
Convective	500 hPa (0000 UTC)	3.4	6.8	7.2	10.2
	500 hPa (1200 UTC)	7.2	6.4	7.6	11.0
Stratiform	500 hPa (0000 UTC)	2.5	3.7	4.0	5.6
	500 hPa (1200 UTC)	4.2	3.1	4.2	6.0

Note: SCB, Sichuan basin; SEC, Southeast China; MEC, middle-eastern China; NWP, Northwest Pacific.

the decreasing magnitude is 0–2 K. Notably, the cooling over the land regions (SCB, SEC, and MEC) is more significant than that over the ocean region (NWP) in the lower troposphere, because of the land surface discrepancy. A positive temperature anomaly causes updraft in the middle troposphere, and the strongest warming occurs at 300 hPa. This is because precipitation releases latent heat (Yang and Smith, 2000), and then the increasing temperature causes divergence that enhances the upward

movement at this level. Compared with Fig. 11, the temperature anomaly for stratiform precipitation shows a similar pattern in Fig. 12. However, a significant positive anomaly for stratiform precipitation occurs higher in the middle troposphere compared with convective precipitation, because latent heat released by stratiform precipitation is mainly concentrated in the upper troposphere (Fu et al., 2003). Stratiform precipitation has the characteristic of longevity. Thus, the decreasing temper-

**Table 6.** Mean convective available potential energy (CAPE;  $J \text{ kg}^{-1}$ ) for convective and stratiform precipitation in the rainy season during 1998–2012 in four regions of East Asia

		SCB	SEC	MEC	NWP
Convective	CAPE (0000 UTC)	2469	3296	2807	3826
	CAPE (1200 UTC)	3260	3385	3064	3097
Stratiform	CAPE (0000 UTC)	2094	2637	2312	2980
	CAPE (1200 UTC)	2473	2741	2548	2738

Note: SCB, Sichuan basin; SEC, Southeast China; MEC, middle-eastern China; NWP, Northwest Pacific.

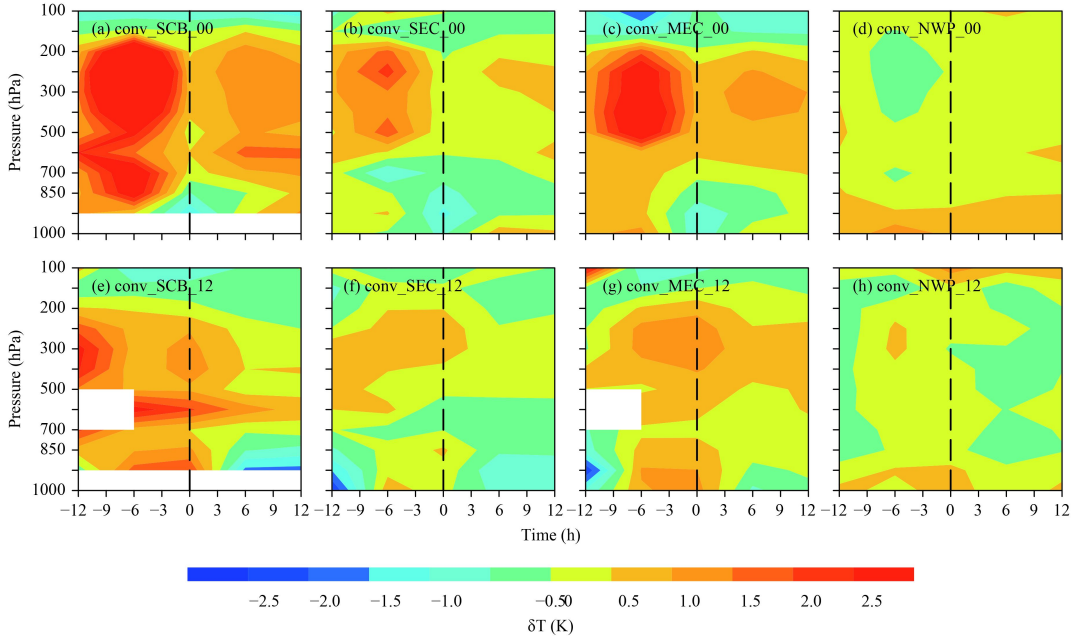


**Fig. 11.** Temperature anomaly calculated from IGRA inside convective precipitating clouds in the rainy season during 1998–2012 in four regions of East Asia (SCB, Sichuan basin; SEC, Southeast China; MEC, middle-eastern China; NWP, Northwest Pacific).

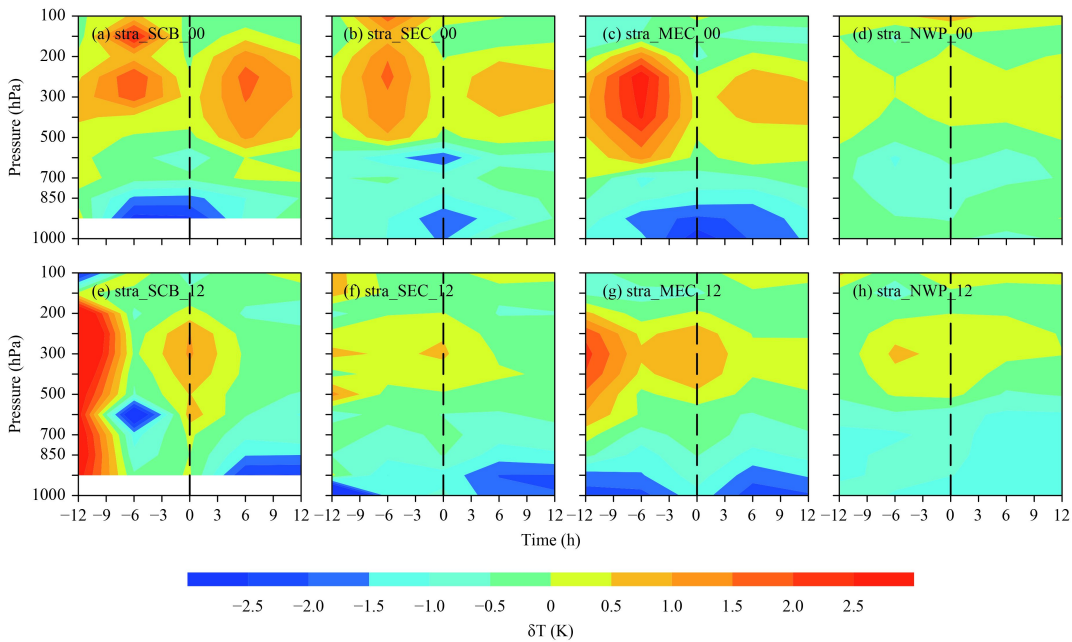


**Fig. 12.** As in Fig. 11, but for stratiform precipitation.

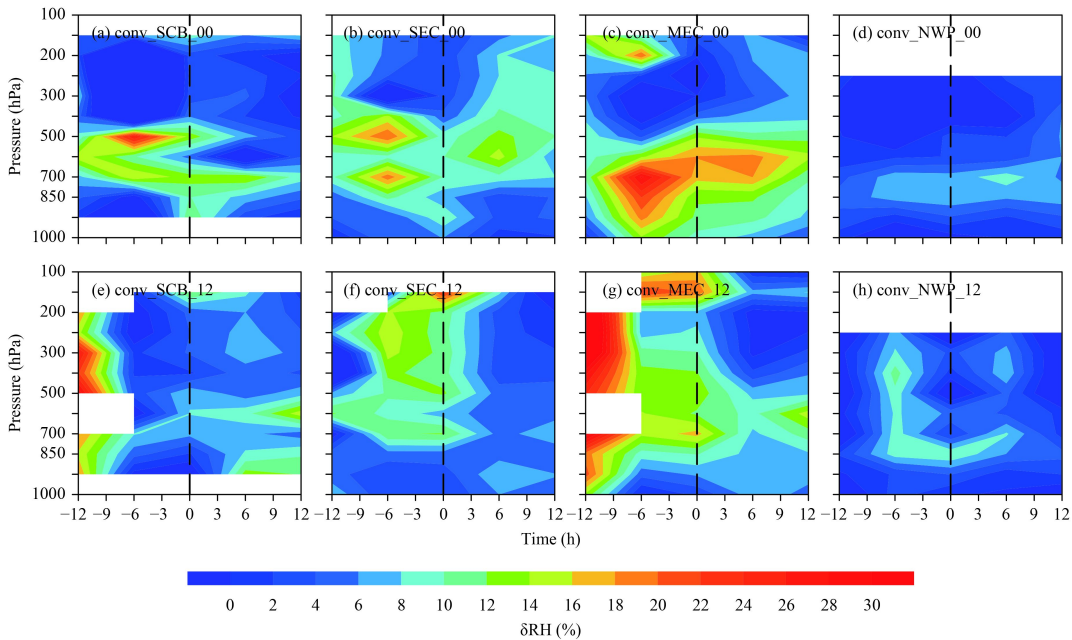
ature anomaly for stratiform precipitation is more significant than that of convective precipitation in the lower

troposphere. In short, the temperature anomaly displays a cooling anomaly in the lower troposphere and warming

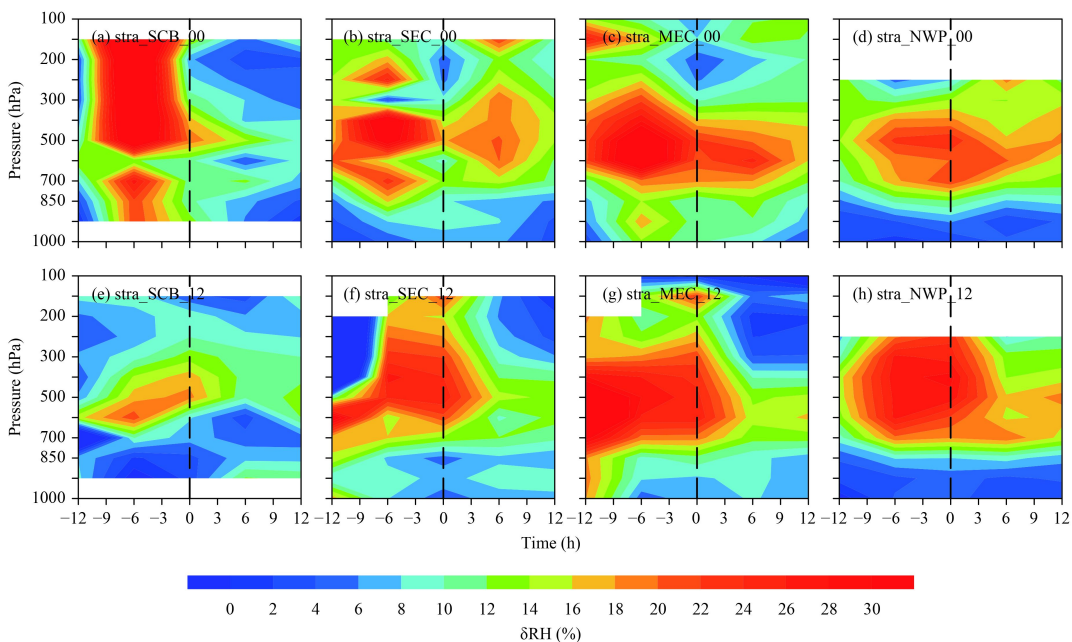
anomaly in the middle troposphere, which is coincident with the latent heating structure and the vertical distribution of temperature reported in previous studies (Tao et al., 2010; Rapp et al., 2011; Mitovski and Folkins, 2014). This temperature anomaly pattern enhances the atmospheric stability in the middle troposphere (Folkins, 2013), which reduces positive buoyancy and inhibits the upward movement of precipitation.

Figure 13 shows a positive relative humidity anomaly

appears 6 h prior to convective precipitation in the middle troposphere (700–500 hPa) in SCB, SEC, and MEC, but not in NWP, because moist convection over land regions is different from that over the ocean (Mitovski et al., 2010). The atmosphere is drier over land areas than over the ocean, and is sensitive to increasing moisture when precipitation occurs. Consequently, the increase in relative humidity over the land regions (SEC, SEC, and MEC) is more significant than that over the



**Fig. 13.** Relative humidity anomaly calculated from IGRA data inside convective precipitating clouds in the rainy season during 1998–2012 in four regions of East Asia (SCB, Sichuan basin; SEC, Southeast China; MEC, middle-eastern China; NWP, Northwest Pacific).



**Fig. 14.** As in Fig. 13, but for stratiform precipitation.

ocean region (NWP). Figure 14 shows that the positive relative humidity anomaly pattern for stratiform precipitation is similar to that for convective precipitation in the middle troposphere, but the increase in relative humidity is more evident than that for convective precipitation. In conclusion, a significant positive relative humidity anomaly appears in the middle troposphere (700–500 hPa) about 6 h prior to precipitation, and the increase in moisture is particularly evident for stratiform precipitation. The positive relative humidity anomaly in the middle troposphere generates negative buoyancy (Mitovski et al., 2010), which suggests that increasing moisture inhibits the vertical extent of stratiform precipitation in the four regions.

#### 4. Summary and conclusions

In this work, a new quasi spatiotemporally synchronized dataset is established based on IGRA and PR 2A25. Using the data, we focus on the link between the vertical structure of precipitation and the thermal characteristics of the atmosphere inside convective and stratiform precipitating clouds in the rainy season of East Asia. This provides an opportunity to better understand the thermal and dynamic processes involved in precipitation, and acts as a reference for the development of weather models. The results can be summarized as follows:

The vertical structure of precipitation shows that convective precipitation has strong vertical movements and develops higher than 10 km. Generally, the radar storm tops for convective precipitation are higher than those for stratiform precipitation. The storm tops over the land regions (SCB, SEC, and MEC) are higher than those over the ocean region (NWP). Besides, the storm tops at 1200 UTC are higher than at 0000 UTC, for both precipitation types, over the land regions (SCB, SEC, and MEC); whereas, the opposite result is found over the ocean region (NWP). In addition, the relationship between the storm tops and near-surface rain rates reveals that the storm tops for convective precipitation increase with an increment in the near-surface rain rate in SEC, MEC, and NWP.

Convective activity develops deeper for convective precipitation than stratiform precipitation in the four regions. Moreover, the atmospheric state is more unstable at 1200 UTC than at 0000 UTC in SCB, SEC, and MEC, which indicates the atmospheric stability is more unstable in the evening over land regions. The opposite result is found in NWP. Combining the results for atmospheric stability and the vertical structure of precipitation, it can be deduced that unstable energy is correlated

with the depth of precipitation development.

Furthermore, the temperature anomaly structures show a cooling anomaly in the lower troposphere and a warming anomaly in the middle troposphere, which would inhibit the vertical development of precipitation. Additionally, the increasing relative humidity is more significant prior to convective and stratiform precipitation in the middle troposphere and could inhibit the vertical extent of precipitation in the four regions.

**Acknowledgments.** We thanks the GSFC for providing the TRMM PR 2A25 data, the NCDC for providing the IGRA data, and the NOAA-CIRES Climate Diagnosis Center for providing the NCEP data. Additionally, we appreciate the constructive suggestions of the two anonymous reviewers.

#### REFERENCES

- Adams, D. K., and E. P. Souza, 2009: CAPE and convective events in the southwest during the North American monsoon. *Mon. Wea. Rev.*, **137**, 83–98, doi: [10.1175/2008MWR2502.1](https://doi.org/10.1175/2008MWR2502.1).
- Alexeev, V. A., I. Esau, I. V. Polyakov, et al., 2012: Vertical structure of recent Arctic warming from observed data and reanalysis products. *Climatic Change*, **111**, 215–239, doi: [10.1007/s10584-011-0192-8](https://doi.org/10.1007/s10584-011-0192-8).
- Bao, X. H., F. Q. Zhang, and J. H. Sun, 2011: Diurnal variations of warm-season precipitation east of the Tibetan Plateau over China. *Mon. Wea. Rev.*, **139**, 2790–2810, doi: [10.1175/MWR-D-11-00006.1](https://doi.org/10.1175/MWR-D-11-00006.1).
- Chen, F. J., Y. F. Fu, P. Liu, et al., 2016: Seasonal variability of storm top altitudes in the tropics and subtropics observed by TRMM PR. *Atmos. Res.*, **169**, 113–126, doi: [10.1016/j.atmosres.2015.09.017](https://doi.org/10.1016/j.atmosres.2015.09.017).
- Ding, Y. H., Z. Y. Wang, and Y. Sun, 2008: Inter-decadal variation of the summer precipitation in East China and its association with decreasing Asian summer monsoon. Part I: Observed evidences. *Int. J. Climatol.*, **28**, 1139–1161, doi: [10.1002/joc.1615](https://doi.org/10.1002/joc.1615).
- Durre, I., R. S. Vose, and D. B. Wuertz, 2006: Overview of the integrated global radiosonde archive. *J. Climate*, **19**, 53–68, doi: [10.1175/JCLI3594.1](https://doi.org/10.1175/JCLI3594.1).
- Feng, S., Y. F. Fu, and Q. N. Xiao, 2012: Trends in the global tropopause thickness revealed by radiosondes. *Geophys. Res. Lett.*, **39**, L20706, doi: [10.1029/2012GL053460](https://doi.org/10.1029/2012GL053460).
- Folkins, I., 2013: The melting level stability anomaly in the tropics. *Atmos. Chem. Phys.*, **13**, 1167–1176, doi: [10.5194/acp-13-1167-2013](https://doi.org/10.5194/acp-13-1167-2013).
- Folkins, I., S. Fueglistaler, G. Lesins, et al., 2008: A low-level circulation in the tropics. *J. Atmos. Sci.*, **65**, 1019–1034, doi: [10.1175/2007JAS2463.1](https://doi.org/10.1175/2007JAS2463.1).
- Fu, Y. F., and G. S. Liu, 2003: Precipitation characteristics in mid-latitude East Asia as observed by TRMM PR and TMI. *J. Meteor. Soc. Jpn. Ser. II*, **81**, 1353–1369, doi: [10.2151/jmsj.81.1353](https://doi.org/10.2151/jmsj.81.1353).
- Fu, Y. F., R. C. Yu, Y. P. Xu, et al., 2003: Analysis on precipitation structures of two heavy rain cases by using TRMM PR

- and IMI. *Acta Meteor. Sinica*, **61**, 421–431, doi: [10.3321/j.issn:0577-6619.2003.04.004](https://doi.org/10.3321/j.issn:0577-6619.2003.04.004). (in Chinese)
- Fu, Y. F., J. Y. Feng, H. F. Zhu, et al., 2005: Structures of a thermal convective precipitation system happened in controlling of the western subtropical Pacific high. *Acta Meteor. Sinica*, **63**, 750–761, doi: [10.3321/j.issn:0577-6619.2005.05.019](https://doi.org/10.3321/j.issn:0577-6619.2005.05.019). (in Chinese)
- Fu, Y. F., R. C. Yu, C. G. Cui, et al., 2007: The structure characteristics of precipitating clouds over the East Asia Based on TRMM measurements. *Torrent. Rain Disast.*, **26**, 9–20. (in Chinese)
- Fu, Y. F., A. M. Zhang, Y. Liu, et al., 2008: Characteristics of seasonal scale convective and stratiform precipitation in Asia based on measurements by TRMM precipitation radar. *Acta Meteor. Sinica*, **66**, 730–746. (in Chinese)
- Fu, Y. F., A. Q. Cao, T. Y. Li, et al., 2012: Climatic characteristics of the storm top altitude for the convective and stratiform precipitation in summer Asia based on measurements of the TRMM precipitation radar. *Acta Meteor. Sinica*, **70**, 436–451, doi: [10.11676/qxb2012.037](https://doi.org/10.11676/qxb2012.037). (in Chinese)
- Fu, Y. F., Q. Liu, Y. Gao, et al., 2013: A feasible method for merging the TRMM microwave imager and precipitation radar data. *J. Quant. Spectr. Radiat. Transf.*, **122**, 155–169, doi: [10.1016/j.jqsrt.2012.08.028](https://doi.org/10.1016/j.jqsrt.2012.08.028).
- Fu, Y. F., X. Pan, Y. J. Yang, et al., 2017: Climatological characteristics of summer precipitation over East Asia measured by TRMM PR: A review. *J. Meteor. Res.*, **31**, 142–159, doi: [10.1007/s13351-017-6156-9](https://doi.org/10.1007/s13351-017-6156-9).
- Guo, Y. J., and Y. H. Ding, 2009: Long-term free-atmosphere temperature trends in China derived from homogenized in situ radiosonde temperature series. *J. Climate*, **22**, 1037–1051, doi: [10.1175/2008JCLI2480.1](https://doi.org/10.1175/2008JCLI2480.1).
- Houze, Jr. R. A., 1997: Stratiform precipitation in regions of convection: A meteorological paradox. *Bull. Amer. Meteor. Soc.*, **78**, 2179–2196, doi: [10.1175/1520-0477\(1997\)078<2179:SPIROC>2.0.CO;2](https://doi.org/10.1175/1520-0477(1997)078<2179:SPIROC>2.0.CO;2).
- Houze, Jr. R. A., D. C. Wilton, and B. F. Smull, 2007: Monsoon convection in the Himalayan region as seen by the TRMM precipitation radar. *Quart. J. Roy. Meteor. Soc.*, **133**, 1389–1411, doi: [10.1002/qj.106](https://doi.org/10.1002/qj.106).
- Iturrioz, I., E. Hernández, P. Ribera, et al., 2007: Instability and its relation to precipitation over the Eastern Iberian Peninsula. *Adv. Geosci.*, **10**, 45–50, doi: [10.5194/adgeo-10-45-2007](https://doi.org/10.5194/adgeo-10-45-2007).
- Juneng, L., and F. T. Tangang, 2005: Evolution of ENSO-related rainfall anomalies in southeast Asia region and its relationship with atmosphere-ocean variations in Indo-Pacific sector. *Climate Dyn.*, **25**, 337–350, doi: [10.1007/s00382-005-0031-6](https://doi.org/10.1007/s00382-005-0031-6).
- Kummerow, C., W. Barnes, T. Kozu, et al., 1998: The tropical rainfall measuring mission (TRMM) sensor package. *J. Atmos. Oceanic Technol.*, **15**, 809–817, doi: [10.1175/1520-0426\(1998\)015<0809:TTRMMT>2.0.CO;2](https://doi.org/10.1175/1520-0426(1998)015<0809:TTRMMT>2.0.CO;2).
- Lang, S., W. K. Tao, J. Simpson, et al., 2003: Modeling of convective-stratiform precipitation processes: Sensitivity to partitioning methods. *J. Appl. Meteor.*, **42**, 505–527, doi: [10.1175/1520-0450\(2003\)042<0505:MOCSPP>2.0.CO;2](https://doi.org/10.1175/1520-0450(2003)042<0505:MOCSPP>2.0.CO;2).
- Li, R., Q. L. Min, X. Q. Wu, et al., 2013: Retrieving latent heating vertical structure from cloud and precipitation profiles—Part II: Deep convective and stratiform rain processes. *J. Quant. Spectr. Radiat. Transf.*, **122**, 47–63, doi: [10.1016/j.jqsrt](https://doi.org/10.1016/j.jqsrt).
- and 2012.11.029.
- Liu, W. B., Z. J. Liu, and C. Luo, 2012: Characteristics of the synoptic time scale variability over the South China Sea based on Tropical Rainfall Measuring Mission. *Meteor. Atmos. Phys.*, **115**, 163–171, doi: [10.1007/s00703-011-0174-4](https://doi.org/10.1007/s00703-011-0174-4).
- Liu, G. S., and Y. F. Fu, 2001: The characteristics of tropical precipitation profiles as inferred from satellite radar measurements. *J. Meteor. Soc. Japan*, **79**, 131–143, doi: [10.2151/jmsj.79.131](https://doi.org/10.2151/jmsj.79.131).
- Liu, P., and Y. F. Fu, 2010: Climatic characteristics of summer convective and stratiform precipitation in southern China based on measurements by TRMM precipitation radar. *Chinese J. Atmos. Sci.*, **34**, 802–814. (in Chinese)
- Liu, P., C. Y. Li, Y. Wang, et al., 2013: Climatic characteristics of convective and stratiform precipitation over the Tropical and Subtropical areas as derived from TRMM PR. *Sci. China Earth Sci.*, **56**, 375–385, doi: [10.1007/s11430-012-4474-4](https://doi.org/10.1007/s11430-012-4474-4).
- Liu, Y. J., Y. H. Ding, and Y. L. Song, 2005: The moisture transport and moisture budget over the south China sea before and after the summer monsoon onset in 1998. *J. Trop. Meteor.*, **21**, 55–62. (in Chinese)
- Lu, D. R., Y. J. Yang, and Y. F. Fu, 2016: Interannual variability of summer monsoon convective and stratiform precipitations in East Asia during 1998–2013. *Int. J. Climatol.*, **36**, 3507–3520, doi: [10.1002/joc.4572](https://doi.org/10.1002/joc.4572).
- Masunaga, H., 2012: A satellite study of the atmospheric forcing and response to moist convection over tropical and subtropical oceans. *J. Atmos. Sci.*, **69**, 150–167, doi: [10.1175/JAS-D-11-016.1](https://doi.org/10.1175/JAS-D-11-016.1).
- Mitovski, T., I. Folkins, K. Von Salzen, et al., 2010: Temperature, relative humidity, and divergence response to high rainfall events in the tropics: Observations and models. *J. Climate*, **23**, 3613–3625, doi: [10.1175/2010JCLI3436.1](https://doi.org/10.1175/2010JCLI3436.1).
- Mitovski, T., and I. Folkins, 2014: Anomaly patterns about strong convective events in the tropics and midlatitudes: Observations from radiosondes and surface weather stations. *J. Geophys. Res.*, **119**, 385–406, doi: [10.1002/2013JD020447](https://doi.org/10.1002/2013JD020447).
- Nesbitt, S. W., and E. J. Zipser, 2003: The diurnal cycle of rainfall and convective intensity according to three years of TRMM measurements. *J. Climate*, **16**, 1456–1475, doi: [10.1175/1520-0442-16.10.1456](https://doi.org/10.1175/1520-0442-16.10.1456).
- Qin, F., and Y. F. Fu, 2016: TRMM-observed summer warm rain over the tropical and subtropical Pacific Ocean: Characteristics and regional differences. *J. Meteor. Res.*, **30**, 371–385, doi: [10.1007/s13351-016-5151-x](https://doi.org/10.1007/s13351-016-5151-x).
- Rapp, A. D., C. D. Kummerow, and L. Fowler, 2011: Interactions between warm rain clouds and atmospheric preconditioning for deep convection in the tropics. *J. Geophys. Res.*, **116**, D23210, doi: [10.1029/2011JD016143](https://doi.org/10.1029/2011JD016143).
- Ratnam, M. V., Y. D. Santhi, M. Rajeevan, et al., 2013: Diurnal variability of stability indices observed using radiosonde observations over a tropical station: Comparison with microwave radiometer measurements. *Atmos. Res.*, **124**, 21–33, doi: [10.1016/j.atmosres.2012.12.007](https://doi.org/10.1016/j.atmosres.2012.12.007).
- Rosenfeld, D., and I. M. Lensky, 1998: Satellite-based insights into precipitation formation processes in continental and maritime convective clouds. *Bull. Amer. Meteor. Soc.*, **79**, 2457–2476, doi: [10.1175/1520-0477\(1998\)079<2457:SBIIPF>2.0.CO;2](https://doi.org/10.1175/1520-0477(1998)079<2457:SBIIPF>2.0.CO;2).

- Schumacher, C., and Jr. R. A. Houze, 2003: Stratiform rain in the tropics as seen by the TRMM precipitation radar. *J. Climate*, **16**, 1739–1756, doi: [10.1175/1520-0442\(2003\)016<1739:SRITTA>2.0.CO;2](https://doi.org/10.1175/1520-0442(2003)016<1739:SRITTA>2.0.CO;2).
- Sheng, P. X., J. T. Mao, J. G. Li, et al., 2003: *Atmospheric Physics*. Peking University Press, Beijing, 522 pp. (in Chinese)
- Tao, W. K., S. Lang, X. P. Zeng, et al., 2010: Relating convective and stratiform rain to latent heating. *J. Climate*, **23**, 1874–1893, doi: [10.1175/2009JCLI3278.1](https://doi.org/10.1175/2009JCLI3278.1).
- Wu, X. K., X. S. Qie, and T. Yuan, 2013: Regional distribution and diurnal variation of deep convective systems over the Asian monsoon region. *Sci. China Earth Sci.*, **56**, 843–854, doi: [10.1007/s11430-012-4551-8](https://doi.org/10.1007/s11430-012-4551-8).
- Xia, J. W., and Y. F. Fu, 2016: The Vertical characteristics of temperature and humidity inside convective and stratiform precipitating clouds in the East Asian summer monsoon region and Indian summer monsoon region. *Chinese J. Atmos. Sci.*, **40**, 563–580, doi: [10.3878/j.issn.1006-9895.1507.15123](https://doi.org/10.3878/j.issn.1006-9895.1507.15123). (in Chinese)
- Xian, T., and Y. F. Fu, 2015: Characteristics of tropopause-penetrating convection determined by TRMM and COSMIC GPS radio occultation measurements. *J. Geophys. Res.*, **120**, 7006–7024, doi: [10.1002/2014JD022633](https://doi.org/10.1002/2014JD022633).
- Xu, W. X., 2013: Precipitation and convective characteristics of summer deep convection over East Asia observed by TRMM. *Mon. Wea. Rev.*, **141**, 1577–1592, doi: [10.1175/MWR-D-12-00177.1](https://doi.org/10.1175/MWR-D-12-00177.1).
- Yang, S., and E. A. Smith, 2000: Vertical structure and transient behavior of convective-stratiform heating in TOGA COARE from combined satellite-sounding analysis. *J. Appl. Meteor.*, **39**, 1491–1513, doi: [10.1175/1520-0450\(2000\)039<1491:VSATBO>2.0.CO;2](https://doi.org/10.1175/1520-0450(2000)039<1491:VSATBO>2.0.CO;2).
- Yu, R. C., T. J. Zhou, A. Y. Xiong, et al., 2007: Diurnal variations of summer precipitation over contiguous China. *Geophys. Res. Lett.*, **34**, L01704, doi: [10.1029/2006GL028129](https://doi.org/10.1029/2006GL028129).
- Yu, R. C., J. Li, H. M. Chen, et al., 2014: Progress in studies of the precipitation diurnal variation over contiguous China. *J. Meteor. Res.*, **28**, 877–902, doi: [10.11676/qxxb2014.047](https://doi.org/10.11676/qxxb2014.047). (in Chinese)
- Yuter, S. E., and Jr. R. A. Houze, 1995: Three-dimensional kinematic and microphysical evolution of Florida cumulonimbus. Part I: Spatial distribution of updrafts, downdrafts, and precipitation. *Mon. Wea. Rev.*, **123**, 1921–1940, doi: [10.1175/1520-0493\(1995\)123<1921:TDKAME>2.0.CO;2](https://doi.org/10.1175/1520-0493(1995)123<1921:TDKAME>2.0.CO;2).
- Zheng, D., Y. J. Zhang, W. T. Lu, et al., 2008: Simulation study about the influence of atmospheric stratification on lightning activities. *Acta Meteor. Sinica*, **22**, 78–90. (in Chinese)
- Zhou, T. J., and Yu, R. C., 2005: Atmospheric water vapor transport associated with typical anomalous summer rainfall patterns in China. *J. Geophys. Res.*, **110**, D08104, doi: [10.1029/2004JD005413](https://doi.org/10.1029/2004JD005413).
- Zhou, L., and Y. Q. Wang, 2006: Tropical Rainfall Measuring Mission observation and regional model study of precipitation diurnal cycle in the New Guinean region. *J. Geophys. Res.*, **111**, D17104, doi: [10.1029/2006JD007243](https://doi.org/10.1029/2006JD007243).
- Zhou, T., R. C. Yu, H. M. Chen, et al., 2008: Summer precipitation frequency, intensity, and diurnal cycle over China: A comparison of satellite data with rain gauge observations. *J. Climate*, **21**, 3997–4010, doi: [10.1175/2008JCLI2028.1](https://doi.org/10.1175/2008JCLI2028.1).
- Zhu, Y. L., H. J. Wang, W. Zhou, et al., 2011: Recent changes in the summer precipitation pattern in East China and the background circulation. *Climate Dyn.*, **36**, 1463–1473, doi: [10.1007/s00382-010-0852-9](https://doi.org/10.1007/s00382-010-0852-9).

Tech & Copy Editor: Zhirong CHEN  
Language Editor: Colin SMITH